A Steady State Continuous Flow Chamber

for the Study of Daytime and Nighttime Chemistry

under Atmospherically Relevant NO levels

Xuan Zhang [1*], John Ortega [1*], Yuanlong Huang [2], Stephen Shertz [1],

Geoffrey S. Tyndall [1], and John J. Orlando [1]

[1] Atmospheric Chemistry Observation & Modeling Laboratory (ACOM), National Center for Atmospheric Research (NCAR), Boulder, CO, USA

[2] Department of Environmental Science and Engineering, California Institute of Technology, Pasadena, CA, USA

[*] Authors contributed equally to this work.

Correspondence to: Xuan Zhang (xuanz@ucar.edu)

1   **Abstract**

2   Experiments performed in laboratory chambers have contributed significantly to the
3   understanding of the fundamental kinetics and mechanisms of the chemical reactions occurring
4   in the atmosphere. Two chemical regimes, classified as 'high-NO' versus 'zero-NO' conditions,
5   have been extensively studied in previous chamber experiments. Results derived from these two
6   chemical scenarios are widely parameterized in chemical transport models to represent key
7   atmospheric processes in urban and pristine environments. As the anthropogenic NO_x emissions
8   in the United States have decreased remarkably in the past few decades, the classic 'high-NO'
9   and 'zero-NO' conditions are no longer applicable to many regions that are constantly impacted
10   by both polluted and background air masses. We present here the development and
11   characterization of the NCAR Atmospheric Simulation Chamber, which is operated in steady
12   state continuous flow mode for the study of atmospheric chemistry under 'intermediate NO'
13   conditions. This particular chemical regime is characterized by constant sub-ppb levels of NO
14   and can be created in the chamber by precise control of the inflow NO concentration and the
15   ratio of chamber mixing to residence timescales. Over the range of conditions achievable in the
16   chamber, the lifetime of peroxy radicals (RO_2), a key intermediate from the atmospheric
17   degradation of volatile organic compounds (VOCs), can be extended to several minutes, and a
18   diverse array of reaction pathways, including unimolecular pathways and bimolecular reactions
19   with NO and HO_2, can thus be explored. Characterization experiments under photolytic and dark
20   conditions were performed and, in conjunction with model predictions, provide a basis for
21   interpretation of prevailing atmospheric processes in environments with intertwined biogenic and
22   anthropogenic activities. We demonstrate the proof of concept of the steady state continuous
23   flow chamber operation through measurements of major first-generation products, methacrolein
24   (MACR) and methyl vinyl ketone (MVK), from OH- and NO_3-initiated oxidation of isoprene.

1. Introduction

25

26   With the discovery of the role of biogenic volatile organic compounds (BVOCs) in urban
27 photochemical smog (Chameides et al., 1988), the interactions of biogenic emissions with man-
28 made pollution and their subsequent impact on the atmosphere's oxidative capacity and aerosol
29 burden have received extensive studies in the ensuing decades (De Gouw et al., 2005; Ng et al.,
30 2007; Goldstein et al., 2009; Surratt et al., 2010; Rollins et al., 2012; Shilling et al., 2013; Xu et
31 al., 2015). A particular research focus has been understanding the influence of nitrogen oxides
32 ($NO_x = NO + NO_2$) on the atmospheric oxidation cascades of BVOCs, which ultimately generate
33 ozone (O_3) and secondary organic aerosols (SOA). Nitrogen oxides alter the distribution of
34 BVOC oxidation products by primarily modulating the fate of peroxy radicals (RO_2), a key
35 intermediate produced from the atmospheric degradation of VOCs by major oxidants including
36 OH, O_3, and NO_3. In the absence of NO_x, RO_2 reacts predominantly with HO_2 radicals yielding
37 organic peroxides and other products, and to a lesser extent, undergoes self/cross-reactions
38 yielding carbonyls, alcohols, and multifunctional species. In the presence of elevated NO_x, the
39 dominant fate of RO_2 is to react with NO leading to ozone production, and also to organic
40 nitrates. During the night, RO_2 also reacts with NO_3 which is produced by the reaction between
41 O_3 and NO_2. In addition, reaction of peroxyacyl radicals ($RC(O)O_2$) with NO_2 produces
42 peroxyacyl nitrates that constitute a large reservoir of reactive nitrogen and a potentially
43 important SOA precursor (Singh and Hanst, 1981; Nguyen et al., 2015).

44   Much of our understanding of the extent to which NO_x mediates the oxidation chemistry of
45 BVOC in the atmosphere has been derived from measurements in laboratory chambers, where
46 two extreme experimental conditions, i.e., 'high NO' vs. 'zero-NO', were mostly performed to
47 examine the reaction pathways of RO_2 radicals (Kroll and Seinfeld, 2008; Orlando and Tyndall,
48 2012; Ziemann and Atkinson, 2012). Results from these two chemical regimes have been widely
49 incorporated into chemical transport models to represent key atmospheric processes in urban and
50 pristine environments, respectively (Kanakidou et al., 2005). In the actual atmosphere, however,
51 the fate of RO_2 radicals is rather more complicated than simply undergoing bimolecular reactions
52 with NO/HO_2 as observed under the two extreme chamber conditions. It has been recently
53 revealed that RO_2 radicals may undergo an internal H-shift followed by sequential O_2 addition,
54 leading to highly oxygenated multifunctional peroxides (Ehn et al., 2014; Jokinen et al., 2015;
55 Kurtén et al., 2015; Kirkby et al., 2016; Zhang et al., 2017). The rate of H-shift largely depends
56 on the thermochemistry of the nascent alkyl radicals and can be reasonably fast, on a time scale
57 of seconds to minutes (Crounse et al., 2013). Further, depending on the stability of the RO_2
58 precursor (alkyl radicals), RO_2 radicals may lose O_2 in competition with bimolecular reactions
59 with NO, NO_3, RO_2, and HO_2. Recent theoretical and laboratory studies have found that the
60 hydroxy peroxy radical conformers produced from isoprene photooxidation decompose readily
61 to allylic radicals on time scales faster than bimolecular processes under atmospherically relevant
62 NO/HO_2 levels (tens to hundreds of parts per trillion by volume). This highly dynamic system
63 leads to formation of distinctly different products that depend on the concentrations of
64 bimolecular reaction partners from those observed in chamber experiments under 'high-NO' and
65 'zero-NO' conditions (Teng et al., 2017).

66   Anthropogenic NO_x emissions in the United States have decreased remarkably in the past
67 few decades (EPA, 2014), resulting in significant changes in the degradation mechanisms of
68 BVOCs, especially in regions impacted by both background and polluted air masses such as the
69 Southeastern United States. However, the ultimate fate of peroxy radicals in environments with

sub-ppb NO levels is still poorly constrained, in part due to a lack of consistent measurements under well controlled conditions. Experimental environments with a controlled NO production at sub-ppb levels have been recently introduced to examine the various RO_2 fates in the atmosphere. For example, a 'slow chemistry' scenario initiated by photolyzing methyl nitrite (CH_3ONO) under extremely low UV intensities as the OH radical source ($J_{CH3ONO} \sim 10^{-5}$ s^{-1}) was created to study the autoxidation chemistry of peroxy radicals produced from isoprene photooxidation (Crounse et al., 2011; Crounse et al., 2012; Teng et al., 2017). The resulting NO and HO_2 mixing ratios are maintained at $\sim$ ppt (parts per trillion by volume) level ($CH_3ONO + O_2 + hv \rightarrow HO_2 + NO + HCHO$) over the course of several hours of reaction, and the average OH concentration (OH $\sim 10^5$ molec cm^{-3}) is approximately one order magnitude lower than that in the typical daytime ambient atmosphere. Another example relates to a recent method development in the Potential Aerosol Mass (PAM) flow tube reactor where nitrous oxide (N_2O) was used to produce $\sim$ ppb (parts per billion by volume) level of NO ($O_3 + hv \rightarrow O_2 + O(^1D)$; $O(^1D) + N_2O \rightarrow 2NO$) (Lambe et al., 2017). Timescales for chemical reactions and gas-particle partitioning are ultimately limited to the mean residence time ($\sim$80 s) of the PAM reactor.

An alternative experimental platform to the batch-mode chamber and flow tube reactor described above is a well-mixed steady-state chamber with continuous feed of reactants and continuous withdrawal of reactor contents (Shilling et al., 2008). An attribute of the continuous flow steady state chamber is that, by control of the inlet reactant concentrations and the ratio of mixing to residence timescales, it is possible to simulate atmospheric oxidation under stable conditions over a wide range of time periods and chemical scenarios. In this study, we present the development and characterization of the NCAR Atmospheric Simulation Chamber, which is operated in steady state continuous flow mode for simulating atmospheric daytime and nighttime chemistry over chemical regimes not accessible in static chamber experiments. We focus on establishing an 'intermediate NO' regime characterized by a constant steady-state NO level ranging from tens of ppt to a few ppb in the chamber. This particular chemical regime is well suited for the study of atmospheric behavior of RO_2 radicals, as they can survive up to minutes and embrace various reaction possibilities as opposed to reaction with NO, NO_3, HO_2, and RO_2 as their dominant fate observed in most batch-mode chamber experiments. We employ the 'intermediate NO' regimes to reexamine the daytime and nocturnal chemistry of isoprene through the measurements of two first-generation products, methacrolein (MACR) and methyl vinyl ketone (MVK).

2. Experimental

2.1 NCAR Atmospheric Simulation Chamber Facilities

The NCAR Atmospheric Simulation Chamber consists of a 10 m^3 FEP Teflon (0.005" thick) bag that is housed in a cubic enclosure with UV reflective surfaces and a bank of 128 wall-mounted blacklight tubes (32W, Type F32T8/BL). To characterize photolytic conditions in the chamber, irradiance spectra were collected in the wavelength range of 180–600 nm at $\sim$0.8 nm resolution by a custom-built spectroradiometer (Petropavlovskikh et al., 2007). Photolysis frequencies were calculated based on the measured downwelling spectral actinic fluxes. The computed photolysis rate of NO_2 ($J_{NO_2} \sim 1.27 \times 10^{-3}$ s^{-1}) agrees within 3% with that measured by photolyzing 18.6 ppb NO_2 in the chamber and monitoring the NO production rate. The chamber is equipped with a standard set of measurements, including an integrated temperature and

113 humidity probe (Model 50U, VAISALA, CO) and a Magnehelic differential pressure indicating
114 transmitter (Model 605-11, Dwyer Instruments, IN). The chamber temperature is controlled at
115 295 K by the building's air conditioning system and increases to 305–306 K under maximum
116 irradiation conditions. The relative humidity of the chamber air is below 10% under dry
117 conditions and can be varied in the range of ~10–50% by flowing a portion of the purified dry
118 flushing air into the chamber through a temperature-controlled water reservoir. The chamber
119 internal pressure is maintained slightly above the ambient pressure to minimize the enclosure air
120 contamination via penetration through the Teflon film.

121 Prior to each experiment, the chamber was flushed with purified dry air from a zero air
122 generator (Model 737, Aadco Instruments, OH) for >12 h until ozone and NO_x levels were below
123 1 ppb. During the operation of the steady state continuous flow mode, the chamber was
124 constantly flushed with purified dry air at 40 L min^{-1}, which gives an average chamber residence
125 time of 4.17 hours. The incoming and outgoing flows were balanced by a feedback control
126 system that maintains a constant internal pressure of $1.2–4.9 \times 10^{-4}$ atm above the ambient. The
127 characteristic mixing time in the chamber was determined to be ~9 min (~4% of the residence
128 time) by rapid injection of tracer compounds including CO_2 and NO. Under such conditions, the
129 gas/particle-phase composition in the outflow can be assumed identical to that in the well-mixed
130 core of the chamber.

131 To mimic daytime photochemistry in the continuous flow mode, steady-state OH mixing
132 ratio was created by photolyzing hydrogen peroxide (H_2O_2) vapor that was continuously flowing
133 into the chamber ($H_2O_2 + h\nu \rightarrow 2OH$, $J_{H_2O_2} \sim 3.93 \times 10^{-7}$ s^{-1}). Specifically, a 20 mL syringe
134 (NORM-JECT, Henke-Sass Wolf, MA) held on a syringe pump (Model 100, kdScientific, MA)
135 kept at ~4 °C was used to deliver H_2O_2 solution (1–30 wt%, Sigma Aldrich, MO) into a glass
136 bulb that was gently warmed at ~32 °C. The liquid delivery rate was sufficiently slow (100–300
137 µL min^{-1}) that all the H_2O_2 vapor was released into the glass bulb through evaporation of a small
138 droplet hanging on the needle tip. An air stream (5 L/min) swept the H_2O_2 vapor into the
139 chamber, resulting in an H_2O_2 mixing ratio in the range of 600 ppb to 16.22 ppm in the injection
140 flow as a function of the concentration of H_2O_2 aqueous solution used. A spreadsheet (Table S2)
141 for calculating the inflow H_2O_2 mixing ratio using the above input method is provided in the
142 Supplement. As H_2O_2-laden air was continuously entering the chamber, it took approximately
143 three turnover times (~12.5 hr) for the desired H_2O_2 vapor mixing ratio to reach steady state in
144 the chamber. The H_2O_2 vapor concentration in the chamber, though not measured, can be
145 estimated from the steady-state OH mixing ratio derived from the observed exponential decay of
146 a given parent hydrocarbon. Constant NO injection flow was achieved by diluting the gas flow
147 from a concentrated NO cylinder (NO = 133.16 ppm, balance N_2) to a desired mixing ratio
148 (0.1–100 ppb) using a set of mass flow controllers (Tylan FC260 and FC262, Mykrolis Corp.,
149 MA). Note that for experiments performed in the absence of any VOC precursor, H_2O_2 and NO
150 were the only two species that were continuously input into the chamber for the establishment of
151 a combination of different photochemical conditions as denoted by the O_3 and NO_x
152 measurements. For the isoprene photooxidation experiments, an isoprene standard (C_5H_8 = 531
153 ppm, balance N_2) was constantly injected into the chamber and diluted with the flushing air to
154 achieve an inflow concentration of ~20 ppb.

155 To mimic the nighttime chemistry in the continuous flow mode, steady-state NO_3 mixing
156 ratio was created by constantly flowing diluted O_3 and NO air into the chamber ($NO+O_3$

157 →NO$_2$+O$_2$; NO$_2$+O$_3$→NO$_3$+O$_2$). The NO source can be replaced by NO$_2$, although the absolute
158 absence of NO does not necessarily represent the actual atmospheric conditions. O$_3$ was
159 produced by photolyzing O$_2$ in air at 185 nm using a mercury "Pen-Ray" lamp (UVP LLC, CA).
160 Ozone concentration in the injection flow can be controlled from 3.5 ppb to 457 ppb
161 automatically by adjusting the mercury lamp duty cycle. To study the RO$_2$+HO$_2$ pathway,
162 formaldehyde (CH$_2$O) was input into the chamber along with NO and O$_3$ to initiate HO$_2$
163 production (NO$_3$+CH$_2$O+O$_2$→HNO$_3$+HO$_2$+CO). Formaldehyde aqueous solution (37 wt%,
164 Sigma Aldrich, MO) was diluted with ultrapure water (Milli-Q, Merck Millipore, MA) to 0.2–1.0
165 wt% and continuously input into the chamber using the same method used for H$_2$O$_2$ input
166 described above. It is worth noting that the formaldehyde aqueous solution contains 10–15%
167 methanol as stabilizer to prevent polymerization. The presence of methanol in the chamber does
168 not significantly impact the nocturnal chemistry as it consumes OH and NO$_3$ radicals to generate
169 formaldehyde and additional HO$_2$ (CH$_3$OH+NO$_3$→HNO$_3$+CH$_2$O+HO$_2$,
170 CH$_3$OH+OH→H$_2$O+CH$_2$O+HO$_2$) (Atkinson et al., 2006). The use of formaldehyde as an HO$_2$
171 source mimics closely the atmospheric nighttime conditions in forest environments (Schwantes
172 et al., 2015). To study the NO$_3$-initiated oxidation of isoprene, an injection flow of diluted
173 isoprene (~10 ppb) was achieved using the procedure described above.

174 **2.2 Analytical measurements**

175 A suite of instruments was used to monitor gas-phase concentrations in the chamber
176 outflow. O$_3$ was monitored by absorption spectroscopy with 0.5 ppb detection limit (Model 49,
177 Thermo Scientific, CO). The O$_3$ monitor was calibrated using an Ozone Primary Standard in the
178 range of 0 to 200 ppb (Model 49i-PS, Thermo Scientific, CO). The O$_3$ monitor used for chamber
179 experiments was periodically checked with the primary standard and was shown to be stable over
180 long periods of time (less than 1 ppb drift in over 1 year). NO was monitored by
181 chemiluminescence with 0.5 ppb detection limit (Model CLD 88Y, Eco Physics, MI). Zero-point
182 and span calibrations of the NO$_x$ monitor were performed prior to each experiment by supplying
183 the instrument with pure N$_2$ gas and diluted NO, respectively. Multi-point calibration was
184 performed on a weekly basis and has shown a good stability and linearity in the NO
185 measurement ranging from 1 ppb to 200 ppb. NO$_x$ (NO+NO$_2$) measurements were performed
186 using a photolytic converter that selectively converts NO$_2$ to NO upstream of the photo-
187 multiplier tube in the CLD 88Y NO monitor. This converter uses two opposing arrays of UV
188 LEDs shining into a cylindrical quartz mixing tube to achieve approximately 50% conversion of
189 NO$_2$ to NO per second. The total efficiency for the equipment described here is approximately
190 70% as determined by measuring calibrated NO$_2$ standards. The sample path always includes
191 the photolytic converter, and typical experiments cycle the power for the LED lights to switch
192 between measuring NO (lights off) and NO$_x$ (lights on). NO$_2$ concentrations were then
193 determined by subtracting the NO from the adjacent NO$_x$ measurements.

194 A customized Proton Transfer Reaction Quadrupole Mass Spectrometer (PTR-Q-MS) was
195 used to measure volatile organic compounds including isoprene (C$_5$H$_8$), methacrolein (MACR,
196 C$_4$H$_6$O), and methyl vinyl ketone (MVK, C$_4$H$_6$O). The instrument was operated at 2.3 mbar drift
197 pressure and 560 V drift voltage. Measurements reported here were obtained at a sampling rate
198 of 10 Hz. In positive-mode operation, a given analyte [M] undergoes proton transfer reaction,
199 producing an ion of the form [M+H]$^+$. The instrument background was collected by sampling the
200 chamber air for at least 30 min prior to each experiment. Measured ion intensities for isoprene
201 (C$_5$H$_9$$^+$, m/z 69) and MACR and MVK (C$_4$H$_7$O$^+$, m/z 71) were calculated as the signal of each ion

202 (counts per seconds) normalized to the total ion signal of H_3O^+. The instrument sensitivities
203 towards isoprene, MACR and MVK were calibrated with a mixture of diluted gas standards. The
204 instrument sensitivity towards MACR is identical to that of MVK, and as a result, the measured
205 $C_4H_7O^+$ signal represents the sum of MACR and MVK in the sampling air. Since artifacts in the
206 measured $C_4H_7O^+$ signal can be produced through thermal decomposition of isoprene oxidation
207 products, such as the peroxides, nitrates, and epoxides, on contact with hot metal surface (Liu et
208 al., 2013; Nguyen et al., 2014; Rivera-Rios et al., 2014), a cold-trap system was used to avoid
209 bias in the interpretation of the PTR-MS data. Specifically, a 1 m section of Teflon tubing was
210 submerged in a low temperature ethanol bath (-40 ± 2 °C) that could trap oxidized products less
211 volatile than the authentic MACR and MVK standards after steady state was established in the
212 chamber. The quantification of the sum of MACR and MVK was then based on the PTR-MS
213 measured $C_4H_7O^+$ (*m/z* 71) signal downstream of the cold-trap.

214 **3. Kinetic Modeling**

215 Reaction kinetics and mechanisms for the gas-phase photochemistry were extracted from the
216 Master Chemical Mechanism (MCMv3.3.1, accessible at http://mcm.leeds.ac.uk/MCM/). The
217 inorganic reaction scheme includes 21 species and 48 reactions; and the isoprene oxidation
218 system includes 611 species and 1974 reactions. The kinetic schemes were implemented in
219 Matlab (Mathworks) to simulate the temporal profile of a given compound *i* in the chamber
220 operated in the steady state continuous flow mode:

$$\frac{dC_i}{dt} \cdot \tau = C_{i,0} + P_i - C_i - \sum k_i \cdot \tau \cdot C_i \qquad \text{(Eq1)}$$

222 where C_i (molec cm^{-3}) is the gas-phase concentration of compound *i* in the well-mixed core of
223 the chamber; $C_{i,0}$ (molec cm^{-3}) is the initial gas-phase concentration of compound *i* in the
224 injection flow; k_i (s^{-1}) is the pseudo-1st-order rate coefficient for a chemical reaction that
225 consumes compound *i*; τ (s) is the chamber mean residence time and can be calculated as the
226 total chamber volume divided by the incoming/outgoing flow rate; and P_i (molec cm^{-3}) is the
227 increment in the concentration of compound *i* through chemical production during one residence
228 time. Note that two terms are neglected in Equation (1), i.e., organic vapor condensation onto
229 particles and deposition on the chamber wall. This is a reasonable simplification here owing to
230 the relatively high volatility ($\geq 10^{-1}$ atm) of compounds studied. Incorporation of these two terms
231 into Equation (1) is feasible given the vapor pressure of compound *i*, suspended particle size
232 distribution, gas-particle and gas-wall partitioning coefficient, accommodation coefficients of
233 compound *i* on particles and walls, and the effective absorbing organic masses on the wall
234 (Zhang et al., 2014a; Zhang et al., 2015b; Huang et al., 2016; McVay et al., 2016; Nah et al.,
235 2016).

236 Model simulations used for comparison with chamber measurements were initialized using
237 experimental conditions summarized in Table S1 in the Supplement. Model input parameters for
238 all simulations include temperature (295 at dark and 306 K under irradiation), local pressure
239 (8.6×10^4 Pa), relative humidity (8% at dark and 5% under irradiation), light intensity
240 (J_{NO_2}= 1.27×10^{-3} s^{-1} under irradiation and 0 at dark), chamber mean residence time (4.17 h), and
241 input mixing ratios of H_2O_2 (0.11−16.2 ppm for photolytic experiments), NO (0.1−100 ppb for
242 photolytic experiments and 10−20 ppb for dark experiments), O_3 (22−225 ppb for dark
243 experiments), HCHO (0−600 ppb for dark experiments), and isoprene (19.9 ppb for photolytic

244 experiments and 10.2 ppb for dark experiments). The model was propagated numerically for 25 h
245 duration for each experiment.

4. Results and Discussions

4.1 Optimal operating conditions for daytime photochemistry

248 Figure 1 shows the model predicted steady-state mixing ratios of OH, HO$_2$, NO$_3$, NO, NO$_2$,
249 and O$_3$ in the chamber after 20 hours of photochemical reactions as a function of the H$_2$O$_2$ and
250 NO concentrations in the continuous injection flow. Six blank chamber experiments were
251 compared with simulations. In general, the model captures the evolution patterns of NO$_x$ and O$_3$
252 well. The predicted mixing ratios of NO, NO$_2$, and O$_3$ agree within 69%, 11%, and 33%,
253 respectively, with the measurements (see Table S1 and Figure S1 in the Supplement). The
254 relatively large NO uncertainties originate from the measurements that were performed close to
255 the instrument detection limit (0.5 ppb).

256 Simulated steady-state mixing ratios of OH radicals ([OH]$_{ss}$) range from ~5×10^5 to ~4×10^6
257 molec cm^{-3}, which over ~4 hours chamber residence time would be roughly equivalent to ~1 h to
258 ~8 h of atmospheric OH exposure (1×10^6 molec cm^{-3}). As expected, [OH]$_{ss}$ increases with
259 increasing NO influxes due to the enhanced NO$_x$/O$_3$ cycling but decreases with increasing H$_2$O$_2$
260 influxes owing to the overwhelming reaction OH+H$_2$O$_2$→H$_2$O+HO$_2$. As a consequence, the
261 steady-state mixing ratios of HO$_2$ radicals ([HO$_2$]$_{ss}$) reach up to ~7×10^9 molec cm^{-3} when 16.2
262 ppm H$_2$O$_2$ is continuously injected into the chamber. If 110 ppb H$_2$O$_2$ is used instead, the
263 resulting [HO$_2$]$_{ss}$ levels fall close to the ambient range (~10^8 molec cm^{-3}).

264 Simulated steady-state NO mixing ratios in the chamber range from ~2 ppt to ~0.9 ppb from
265 combinations of 0.1−20 ppb NO and 0.11−16.22 ppm H$_2$O$_2$ in the injection flow. The ratio of
266 inflow NO concentration to the steady-state NO concentration in the chamber ranges from 5 to
267 93, demonstrating the importance of chemical removal in controlling the overall steady-state NO
268 levels. O$_3$ accumulation is an inevitable consequence under photolytic conditions and, for
269 example, the presence of 10 ppb O$_3$ leads to the chemical removal term ($k_{O_3+NO} \cdot [O_3] \cdot \tau$) in
270 Equation (1) that reduces the steady-state NO concentration by a factor of 60. It is worth noting
271 that under all simulated conditions in the continuous flow mode, O$_3$ (~1−126 ppb) coexists with
272 NO (~0.002−0.9 ppb). This particular chemical scenario, which is impossible to achieve in
273 batch-mode reactors due to prompt conversion of NO to NO$_2$, could then be used to mimic
274 ambient ozonolysis chemistry, for example, in forest regions that frequently encounter polluted
275 air masses from nearby urban areas. The steady-state mixing ratios of NO$_2$ ([NO$_2$]$_{ss}$) exhibit a
276 strong linear correlation with NO influxes. The use of less than 20 ppb NO in the injection flow
277 results in a few to tens of ppb [NO$_2$]$_{ss}$ that is higher than the range typically found in the ambient.
278 The potential 'quenching' effect of NO$_2$ on RO$_2$ radicals through reversible termolecular
279 reactions is discussed shortly.

280 In the so-called 'high-NO$_x$' chamber experiments, the NO$_3$ radical is an unavoidable side-
281 product when black lights are used as a representative of the solar radiation in mimicking the
282 daytime photochemistry in the troposphere. The photolysis of NO$_3$, although its primary sink in
283 the atmosphere, proceeds rather slowly (J_{NO_3}~ 1.8×10^{-3} s^{-1}) under the present chamber
284 photolytic conditions, thereby leading to a significant accumulation of NO$_3$ radicals
285 (7.9×10^4−2.8×10^8 molec cm^{-3}) at steady state. The simulated NO$_3$/OH ratio dictates the extent to

286 which the NO_3 (nighttime) chemistry competes with the OH-initiated (daytime) photochemistry.
287 For compounds that are highly reactive towards NO_3 such as isoprene, NO_3-initiated oxidation
288 accounts for up to ~60% of the overall isoprene degradation pathways at the highest NO_3/OH
289 ratio (~255) simulated. Low concentrations of NO (< 20 ppb) and H_2O_2 (< 2 ppm) in the
290 injection flow are therefore necessary to limit the interferences of NO_3-initiated chemistry.
291 Again, taking isoprene as an example, the NO_3 oxidation pathway contributes less than 0.1% of
292 the overall isoprene degradation kinetics at the lowest NO_3/OH ratio (~0.13) simulated here.

293 Also given in Figure 1 is the calculated lifetime (τ_{RO_2}) of an RO_2 radical with respect to
294 reactions with NO and HO_2 at 306 K. In most batch-mode chamber experiments, τ_{RO_2} of only
295 several seconds or less can be achieved, due to the presence of tens to hundreds of ppb levels of
296 NO and HO_2. Here τ_{RO_2} could extend to 60 s or even longer with the continuous input of low
297 mixing ratios of H_2O_2 ($\leq$ 110 ppb) and NO ($\leq$ 0.2 ppb). Note that the presence of tens of ppb
298 NO_2 in the chamber might impose a 'quenching' effect on the steady state RO_2 level through
299 rapid reversible reactions ($RO_2+NO_2+M\leftrightarrow RO_2NO_2+M$). We evaluate this potential 'quenching
300 effect' using ethylperoxy radical ($C_2H_5O_2$) generated from OH-oxidation of ethane as an
301 example. Simulations shown in Figure S2 in the Supplement reveal that incorporation of the
302 $C_2H_5O_2+NO_2+M\leftrightarrow C_2H_5O_2NO_2+M$ reaction into the mechanism in the presence of ~1−80 ppb
303 NO_2 does not notably change the behavior of $C_2H_5O_2$ radical. One exception is the peroxyacyl
304 radical, which combines with NO_2 yielding peroxyacyl nitrate. For example, under 0.1−16 ppb
305 $[NO_2]_{ss}$ as displayed in Figure 1, we calculate that the time needed for peroxyacetyl radical
306 ($CH_3C(O)O_2$)   to   reach   equilibrium   with   peroxyacetyl   nitrate
307 ($CH_3C(O)O_2+NO_2+M\leftrightarrow CH_3C(O)O_2NO_2+M$) ranges from ~1 to ~10 s, suggesting that the
308 lifetime of peroxyacyl radicals is ultimately controlled by NO_2 instead of NO/HO_2 in the reaction
309 system, and consequently, peroxyacyl radicals are not expected to be long-lived in the current
310 chamber configuration.

311 **4.2 Application to OH-initiated oxidation of isoprene**

312 Methacrolein (MACR) and methyl vinyl ketone (MVK) are major first-generation products
313 from the OH-initiated oxidation of isoprene in the presence of NO (Wennberg et al., 2017). They
314 are produced from the decomposition of β-ISOPO alkoxy radicals that are primarily formed from
315 the reaction of β-ISOPOO peroxy radicals (β-1-OH-2-OO and β-4-OH-3-OO) with NO, see
316 mechanisms displayed in Figure 2 (A). Reactions of β-ISOPOO peroxy radicals with HO_2 and
317 RO_2 also partially yield β-ISOPO alkoxy radicals that ultimately lead to MACR and MVK,
318 although these pathways are considered to be minor in the presence of hundreds to thousands of
319 ppt NO in the atmosphere. The molar yields determined from previous studies range from
320 30−35% for MVK and 20−25% for MACR under high NO conditions (NO > 60 ppb) (Tuazon
321 and Atkinson, 1990; Paulson and Seinfeld, 1992; Miyoshi et al., 1994; Ruppert and Becker,
322 2000; Galloway et al., 2011). It has been recently shown that the six hydroxyl peroxy radicals
323 (ISOPOO) produced from the initial OH addition to the double bonds of isoprene undergo rapid
324 interconversion by removal/addition of O_2 that competes with bimolecular reactions under
325 atmospherically relevant NO levels (Peeters et al., 2014; Teng et al., 2017). As a result, the
326 distribution of ISOPOO radical isomers and their subsequent reaction products varies with their
327 lifetimes with respect to bimolecular reactions. In the presence of hundreds of ppb NO as done
328 by most previous experimental studies, the reaction of ISOPOO radicals with NO dominates over
329 their interconversion, and the production of β-ISOPOO peroxy radical is less favored, leading

330   the experiments to underestimate the MACR and MVK yields typically obtained in ambient
331   conditions. Measurements by Liu et al. (2013) conducted at NO concentrations comparable to
332   the urban environment (~1 ppb) found much higher MACR (~31.8%) and MVK (~44.5%) yields
333   than other previous studies.

334   Here we perform a steady-state continuous-mode experiment to measure the production of
335   MACR and MVK from the OH-initiated oxidation of isoprene in the presence of ~0.45 ppb NO.
336   Figure 3 shows the observed and simulated temporal profiles of NO_x, O_3, C_5H_8, and C_4H_6O over
337   24 hours photooxidation of isoprene. In this experiment, C_5H_8, H_2O_2, and NO were continuously
338   fed into the chamber, with constant inflow concentrations of 19.9 ppb, 600 ppb, and 19 ppb,
339   respectively. An outgoing flow at 40 L min^{-1} continuously withdrew air from the chamber to
340   balance the pressure. After approaching steady state, the sampling tube was submerged into an
341   ethanol low temperature bath (−40±2 °C) to trap oxidized products that would otherwise undergo
342   thermal decomposition introducing interferences in the $C_4H_7O^+$ (*m/z* 71) signal. The measured
343   concentrations of C_5H_8 and C_4H_6O upon cold-trapping agree within 2.8% and 4.6% uncertainties
344   with the model simulations, see Fig.3 (C) and (D).

345   To calculate the total molar yield ($Y_{C_4H_6O}$) of MACR and MVK, two reactions are
346   considered:

347                           $C_5H_8 + OH \xrightarrow{k_1} Y_{C_4H_6O} \cdot C_4H_6O + products$ (R1)

348                               $C_4H_6O + OH \xrightarrow{k_2} products$ (R3)

349   where k_1 is the rate constant for OH reaction with isoprene, and k_2 is taken as the average of rate
350   constants for OH reactions with MACR and MVK. Uncertainties associated with the
351   simplification of k_2 in calculating the MACR and MVK yields will be discussed shortly. Also
352   note that the ozonolysis and NO_3-initiated oxidation in total account for less than 6% of isoprene
353   degradation pathway under current experimental conditions and are neglected in the calculation.

354   In the continuous-mode operation, two mass conservation equations are satisfied at steady
355   state:

356       $$\frac{d[C_5H_8]_{ss}}{dt} = [C_5H_8]_0/\tau - [C_5H_8]_{ss}/\tau - k_1 \cdot [OH]_{ss} \cdot [C_5H_8]_{ss} = 0$$ (Eq2)

357   $$\frac{d[C_4H_6O]_{ss}}{dt} = Y_{C_4H_6O} \cdot k_1 \cdot [OH]_{ss} \cdot [C_5H_8]_{ss} - k_2 \cdot [OH]_{ss} \cdot [C_4H_6O]_{ss} - [C_4H_6O]_{ss}/\tau = 0$$ (Eq3)

358   where $[C_5H_8]_{ss}$ and $[C_4H_6O]_{ss}$ are the PTRMS measured steady-state concentrations of isoprene
359   and the sum of MACR and MVK when using the cold trap, respectively, $[C_5H_8]_0$ is the initial
360   concentration of isoprene, and τ is the chamber mean residence time and can be calculated as the
361   total chamber volume divided by the incoming/outgoing flow rate. The steady state OH radical
362   concentration ($[OH]_{ss}$) can be derived by solving Equation (2). The calculated $[OH]_{ss}$ (3.13×10^6
363   molec cm^{-3}) is 12% higher than the model prediction (2.74×10^6 molec cm^{-3}). The molar yield of
364   the sum of MACR and MVK from isoprene OH oxidation pathway in the presence of ~0.45 ppb
365   NO is thus given by Equation (4) and calculated as 76.7±5.8%:

366       $$Y_{C_4H_6O} = \frac{[C_4H_6O]_{ss} + k_2 \cdot [OH]_{ss} \cdot \tau \cdot [C_4H_6O]_{ss}}{k_1 \cdot [OH]_{ss} \cdot \tau \cdot [C_5H_8]_{ss}} \times f_{\beta\text{-ISOPOO+NO}}$$ (Eq4)

367 Here a 5.8% uncertainty originates from the assumption that MACR+OH and MVK+OH
368 proceed with equal reaction rate, although the rate constant for MVK+OH is ~31% lower than
369 that of MACR+OH. Another potential uncertainty relates to the accuracy of the simulated steady
370 state HO_2 and RO_2 concentrations and the contribution of β-ISOPOO+HO_2 and β-ISOPOO+RO_2
371 reaction pathways to the overall β-ISOPOO fate. The fraction of β-ISOPOO radicals that reacts
372 with NO ($f_{\beta\text{-ISOPOO+NO}}$) was predicted as 0.88, which was used here to scale the final
373 MACR+MVK yield, see Eq(4).

374   In summary, the measured yield of the sum of MACR and MVK in this study is close to that
375 reported by Liu et al. (2013), but ~27–52% higher than the majority of previous measurements
376 performed under high NO conditions (NO > 60 ppb). This is consistent with the dynamic nature
377 of the six ISOPOO radical isomers that undergo rapid interconversion by addition/removal of O_2.
378 In the presence of ~0.45 ppb NO as performed in this study, lifetimes of the β-1-OH-2-OO
379 peroxy radical with respect to reaction with NO and loss of O_2 are estimated as 9.4 s and 0.2 s,
380 respectively, implying that the rapid interconversion between β-ISOPOO and δ-ISOPOO
381 radicals essentially governs their distribution, and under such conditions, the production of
382 thermodynamically more stable β-ISOPOO isomers is favored, leading to higher yields of
383 MACR and MVK. Here the reported MACR and MVK yield from isoprene OH oxidation in the
384 presence of ~0.45 ppb NO represents an illustration of chamber operation at steady state
385 continuous flow mode for the establishment of certain experimental conditions that are not easily
386 accessible from traditional batch-mode chamber experiments. A complete measurement of first-
387 generation oxidation products from isoprene OH reaction under a wide range of NO levels
388 (ISOPOO bimolecular lifetimes) will be forthcoming in a future publication.

389   **4.3 Optimal operating conditions for nighttime chemistry**

390   Figure 4 shows the model simulated steady-state mixing ratios of HO_2, NO_3, NO, NO_2, and
391 O_3 after 16 hours of dark reactions in the chamber as a function of the HCHO concentration and
392 O_3/NO ratio in the continuous chamber inflow. Blank experiments were compared with
393 simulations in five cases (see Table S1 in the Supplement). The model captures the evolution
394 patterns of NO_x and O_3 well. The observed mixing ratios of NO_2 and O_3 agree with the
395 simulations to within 11% and 6%, respectively (Figure S3 in the Supplement).

396   Compared with the photochemical reaction schemes discussed earlier, the nocturnal
397 chemistry is rather straightforward; that is, the inflow O_3/NO ratio governs the steady-state
398 concentrations of NO_3, NO_x, and O_3, while the inflow HCHO concentration ultimately controls
399 the steady-state HO_2 level. Increasing the O_3/NO ratio from 1 to 9 in the continuous inflow leads
400 to increased NO_3 from 2.4×10^5 to 1.1×10^9 molec cm^{-3}, but decreased NO from 1.8 ppb to 20 ppt
401 and decreased NO_2 from 18 to 7 ppb. At a fixed inflow O_3/NO ratio, doubling the NO and O_3
402 concentrations leads to elevated NO_3, NO_x, and O_3 by a factor of 2.0–3.2, 1.5–2.0, and 1.4–2.0,
403 respectively. The use of HCHO as an effective dark HO_2 source does not significantly impact the
404 steady-state mixing ratios of NO_x and O_3, but slightly weakens the NO_3 production.

405   The calculated RO_2 lifetime (τ_{RO_2}) with respect to reactions with NO, NO_3, and HO_2 at 295
406 K ranges from 3 to 225 s. The highest τ_{RO_2} was achieved in the absence of any HCHO source
407 and corresponds to a chemical regime that can be employed to study the intramolecular
408 isomerization (autoxidation) pathway of RO_2 radicals, if any. Adding a continuous flow of
409 HCHO to the system leads to the production of 10^7–10^9 molec cm^{-3} HO_2 radicals that then

410   constitute a significant sink of RO$_2$ radicals and represents prevailing forest environments during
411   nighttime.

4.4 Application to NO$_3$-initiated oxidation of isoprene

413   NO$_3$-initiated oxidation of isoprene proceeds by the NO$_3$ addition to the carbon double
414   bonds followed by O$_2$ addition, yielding six distinct nitrooxy peroxy radicals (INOO), including
415   two isomers (β-INOO) with O$_2$ added on the β-carbon to the nitrate group (see Figure 2B for
416   schematic illustration). The β-INOO radicals react further with NO$_3$, HO$_2$, NO, and RO$_2$,
417   producing nitrooxy alkoxy radicals (β-INO) with molar yields of 1.00, 0.53, 0.97, and 0.40,
418   respectively (Wennberg et al., 2017). The further decomposition of β-INO radicals produces
419   MACR and MVK, together with HCHO and NO$_2$. Depending on the actual fate of β-INOO
420   radicals, the yields of β-INO radicals can then vary from 0.4 to 1.0, resulting in a distinct
421   distribution of final oxidation products. It is thus important to specify the ultimate fate of INOO
422   radicals during quantification of oxidation products from isoprene reaction with NO$_3$. As an
423   illustration, we performed one continuous mode experiment that targets on controlling the
424   steady-state fate of INOO radicals to be their reaction with NO and HO$_2$ (46% and 38% INOO
425   radicals are predicted to react with NO and HO$_2$, respectively, as shown in Fig.5). Note that by
426   adjusting the concentrations and fractions of inflow reactants (O$_3$, NO, HCHO, and C$_5$H$_8$),
427   different chemical fates and lifetimes of INOO radicals can be achieved.

428   Figure 5 shows the observed and predicted temporal profiles of NO$_x$, O$_3$, C$_5$H$_8$, and C$_4$H$_6$O
429   over 25 hours of isoprene oxidation by NO$_3$, with continuous input of 10.2 ppb C$_5$H$_8$, 205 ppb
430   O$_3$, and 59 ppb NO into the chamber and a balancing outgoing flow at 40 L min^{-1} carrying well-
431   mixed reactants and products. It took >16 hours to reach steady state for all the species
432   displayed. In general, the model captures the trends of O$_3$ and NO well, while underpredicting
433   the steady state NO$_2$ by ~26%. After ~18 hours of dark reaction, the PTR-MS sampling tubing
434   was submerged into an ethanol cold bath (− 40±2 °C) to trap artifacts in the PTR-MS measured
435   C$_4$H$_7$O$^+$ (*m/z* 71) signal. The simulated steady-state concentration of isoprene agrees within 9%
436   with the measurements. The derived concentration of the sum of MACR and MVK from the
437   measured C$_4$H$_7$O$^+$ ion intensity upon cold-trapping is ~1.1 ppb, which is ~129% higher than the
438   model predictions (~0.48 ppb). This disagreement can be attributed, to a large extent, to the
439   oversimplified representation of the six different INOO radicals as one δ-INOO isomer in the
440   MCMv3.3.1 mechanism. As a result, the production of β-INOO radical, the important precursor
441   of MACR and MVK, from NO$_3$-initiated oxidation of isoprene is suppressed in the simulations.
442   The measured molar yield of the sum of MACR and MVK is 36.3±12.1%, with uncertainties
443   arising from the fact that 10.5% isoprene is predicted to react with OH as an additional source of
444   MACR and MVK. Using this value, the fraction of β-INOO over the sum of nitrooxy peroxy
445   radicals is estimated as 48.6±16.2%, which is close to that (~46.3%) reported by Schwantes et al.
446   (2015), although the estimated bimolecular lifetime of INOO radical in that study (~30 s) is
447   lower than that predicted in the present work (~50 s). As discussed above, the hydroxyl peroxy
448   radicals produced from OH-oxidation of isoprene could undergo rapid interconversion through
449   addition/removal of O$_2$ at atmospherically relevant lifetimes. This interconversion significantly
450   impacts the subsequent chemistry of individual ISOPOO radical isomers in terms of reaction
451   rates and product distributions. It is likely that the INOO radicals follow similar interconversion
452   due to the small R-OO bond dissociation energy, although no experimental evidence exists. A
453   full examination of the INOO chemistry, i.e., their kinetic and thermodynamic properties as well

454 as their chemical fate at different lifetimes, will be the focus of future studies using this
455 continuous flow chamber operation method.

5. Conclusions

457   We report here the development and characterization of the NCAR Atmospheric Simulation
458 Chamber operated at steady state continuous flow mode for simulating daytime and nocturnal
459 chemistry under atmospherically relevant NO levels. The chamber is designed to achieve a well-
460 controlled steady-state environment by continuous inflow of reactants and continuous
461 withdrawal of reactor contents. We use a combination of kinetic modeling and chamber
462 experiments to characterize the 'intermediate-NO' chemical regime (tens of ppt to a few ppb)
463 that can be achieved by precisely controlling the inlet reactant concentrations and the
464 mixing/residence timescales of the chamber.

465   To mimic daytime photochemistry, continuous input of H_2O_2 and NO gases is required,
466 resulting in steady state OH mixing ratios of $10^5–10^6$ molec cm^{-3} under irradiation. Under such
467 conditions, the lifetime of a peroxy radical with respect to reaction with NO and HO_2 can be
468 extended to 60 s or even longer, thus providing a unique environment to study all reaction
469 possibilities of RO_2 radicals including the intramolecular isomerization (autoxidation) pathway.
470 When studying OH-initiated chemistry, care needs to be taken to avoid a range of experimental
471 conditions (e.g., inflow $H_2O_2 > 2$ ppm and NO > 20 ppb) where NO_3-oxidation might account for
472 a large fraction of the overall degradation pathway of certain parent hydrocarbons such as
473 alkenes.

474   To mimic nighttime chemistry, continuous input of NO (or NO_2) and O_3 is needed to
475 produce steady state NO_3 radicals in the range of $10^6–10^9$ molec cm^{-3} in the dark. Under such
476 conditions, an RO_2 radical can live up to 4 min prior to finding a bimolecular reaction partner
477 (e.g., NO, NO_3, and HO_2), which were the dominant fates of RO_2 radicals in most batch-mode
478 chamber experiments. Again, the long lifetime of RO_2 radicals achieved by the steady state
479 continuous mode operation opens an avenue for close examination of RO_2 unimolecular
480 (isomerization) pathways in nocturnal environments.

481   In simulating both daytime and nighttime chemistry with continuous flow operation method,
482 O_3 accumulation is unavoidable. The extent to which ozonolysis interferes with OH- or NO_3-
483 initiated oxidation chemistry depends on the steady state O_3 concentration achieved in the
484 chamber and its reactivity towards various parent VOCs. Taking isoprene as an example,
485 ozonolysis accounts for $<1\%$ and $<0.1\%$ of the overall isoprene degradation kinetics,
486 respectively, under established steady-state photolytic and dark conditions described above.

487   In atmospheric chemistry, the terms 'zero-NO' versus 'high-NO' have been widely used to
488 classify photooxidation conditions and delineate the gas-phase fate of the peroxy radicals (RO_2)
489 generated from VOCs oxidation (Cappa et al., 2013; Zhang and Seinfeld, 2013; Loza et al.,
490 2014; Schilling Fahnestock et al., 2014; Zhang et al., 2014b; Krechmer et al., 2015; Nguyen et
491 al., 2015; Zhang et al., 2015a; Riva et al., 2016; Schwantes et al., 2017). In the so-called 'high-
492 NO' regime, reaction with NO dominates the fate of RO_2 radicals, whereas in the 'zero-NO'
493 regime, the RO_2 radicals primarily undergo reaction with HO_2 and, perhaps to a much lesser
494 degree, self/cross-combination. The importance of the 'intermediate-NO' regime lies in the fact
495 that at sub-ppb levels of NO, the RO_2+NO and RO_2+HO_2 reactions are expected to co-exist and
496 the RO_2 radical could survive up to several minutes before encountering a partner (NO/HO_2) for

bimolecular reactions. Under such conditions, the RO_2 radical isomers may undergo interconversion by addition/removal of O_2 and intramolecular isomerization (autoxidation) through H-shift. Here we use isoprene as an illustrative VOC to explore the fate of RO_2 radicals under sub-ppb NO. Future work will focus on detailed characterization of oxidation products from isoprene day- and nighttime chemistry with particular attention given to the controlled RO_2 fates and lifetimes.

Data Availability

Data presented in this manuscript are available upon request to the corresponding author.

Competing interests

The authors declare that they have no conflict of interest.

Acknowledgement

The National Center for Atmospheric Research is operated by the University Corporation for Atmospheric Research, under the sponsorship of the National Science Foundation.

Reference:

Atkinson, R., Baulch, D. L., Cox, R. A., Crowley, J. N., Hampson, R. F., Hynes, R. G., Jenkin, M. E., Rossi, M. J., Troe, J., and Subcommittee, I.: Evaluated kinetic and photochemical data for atmospheric chemistry: Volume II–gas phase reactions of organic species, Atmos. Chem. Phys., 6, 3625-4055, 2006.

Cappa, C. D., Zhang, X., Loza, C. L., Craven, J. S., Lee, Y. D., and Seinfeld, J. H.: Application of the Statistical Oxidation Model (SOM) to Secondary Organic Aerosol formation from photooxidation of C_ (12) alkanes, Atmos. Chem. Phys., 13, 1591-1606, 2013.

Chameides, W. L., Lindsay, R. W., Richardson, J., and Kiang, C. S.: The role of biogenic hydrocarbons in urban photochemical smog: Atlanta as a case study, Science, 241, 1473-1476, 1988.

Crounse, J. D., Paulot, F., Kjaergaard, H. G., and Wennberg, P. O.: Peroxy radical isomerization in the oxidation of isoprene, Phys. Chem. Chem. Phys., 13, 13607-13613, 2011.

Crounse, J. D., Knap, H. C., Ørnsø, K. B., Jørgensen, S., Paulot, F., Kjaergaard, H. G., and Wennberg, P. O.: Atmospheric fate of methacrolein. 1. Peroxy radical isomerization following addition of OH and O2, J. Phys. Chem. A, 116, 5756-5762, 2012.

Crounse, J. D., Nielsen, L. B., Jørgensen, S., Kjaergaard, H. G., and Wennberg, P. O.: Autoxidation of organic compounds in the atmosphere, J. Phys. Chem. Lett., 4, 3513-3520, 2013.

De Gouw, J. A., Middlebrook, A. M., Warneke, C., Goldan, P. D., Kuster, W. C., Roberts, J. M., Fehsenfeld, F. C., Worsnop, D. R., Canagaratna, M. R., and Pszenny, A. A. P.: Budget of organic carbon in a polluted atmosphere: Results from the New England Air Quality Study in 2002, J. Geophys. Res. Atmos., 110, 2005.

532 Ehn, M., Thornton, J. A., Kleist, E., Sipilä, M., Junninen, H., Pullinen, I., Springer, M., Rubach,
533 F., Tillmann, R., and Lee, B.: A large source of low-volatility secondary organic aerosol, Nature,
534 506, 476-479, 2014.

535 EPA: Data from the 2011 National Emissions Inventory, Version 1. Accessed 2014.
536 https://http://www.epa.gov/air-emissions-inventories/2011-national-emissions-inventory-nei-
537 data., 2014.

538 Galloway, M. M., Huisman, A. J., Yee, L. D., Chan, A. W. H., Loza, C. L., Seinfeld, J. H., and
539 Keutsch, F. N.: Yields of oxidized volatile organic compounds during the OH radical initiated
540 oxidation of isoprene, methyl vinyl ketone, and methacrolein under high-NOx conditions,
541 Atmos. Chem. Phys., 11, 10779-10790, 2011.

542 Goldstein, A. H., Koven, C. D., Heald, C. L., and Fung, I. Y.: Biogenic carbon and
543 anthropogenic pollutants combine to form a cooling haze over the southeastern United States,
544 Proc. Natl. Acad. Sci. USA, 106, 8835-8840, 2009.

545 Huang, D. D., Zhang, X., Dalleska, N. F., Lignell, H., Coggon, M. M., Chan, C. M., Flagan, R.
546 C., Seinfeld, J. H., and Chan, C. K.: A note on the effects of inorganic seed aerosol on the
547 oxidation state of secondary organic aerosol—α-pinene ozonolysis, J. Geophys. Res. Atmos.,
548 2016.

549 Jokinen, T., Berndt, T., Makkonen, R., Kerminen, V.-M., Junninen, H., Paasonen, P., Stratmann,
550 F., Herrmann, H., Guenther, A. B., and Worsnop, D. R.: Production of extremely low volatile
551 organic compounds from biogenic emissions: Measured yields and atmospheric implications,
552 Proc. Natl. Acad. Sci. USA, 112, 7123-7128, 2015.

553 Kanakidou, M., Seinfeld, J. H., Pandis, S. N., Barnes, I., Dentener, F. J., Facchini, M. C.,
554 Dingenen, R. V., Ervens, B., Nenes, A., and Nielsen, C. J.: Organic aerosol and global climate
555 modelling: a review, Atmos. Chem. Phys., 5, 1053-1123, 2005.

556 Kirkby, J., Duplissy, J., Sengupta, K., Frege, C., Gordon, H., Williamson, C., Heinritzi, M.,
557 Simon, M., Yan, C., and Almeida, J.: Ion-induced nucleation of pure biogenic particles, Nature,
558 533, 521-526, 2016.

559 Krechmer, J. E., Coggon, M. M., Massoli, P., Nguyen, T. B., Crounse, J. D., Hu, W., Day, D. A.,
560 Tyndall, G. S., Henze, D. K., Rivera-Rios, J. C., Nowak, J. B., Kimmel, J. R., III, R. L. M.,
561 Stark, H., Jayne, J. T., Sipila, M., Junninen, H., Clair, J. M. S., Zhang, X., Feiner, P. A., Zhang,
562 L., Miller, D. O., Brune, W. H., Keutsch, F. N., Wennberg, P. O., Seinfeld, J. H., Worsnop, D.
563 R., Jimenez, J. L., and Canagaratna, M. R.: Formation of low volatility organic compounds and
564 secondary organic aerosol from isoprene hydroxyhydroperoxide low-NO oxidation, Environ. Sci.
565 Technol., 49, 10330-10339, 2015.

566 Kroll, J. H., and Seinfeld, J. H.: Chemistry of secondary organic aerosol: Formation and
567 evolution of low-volatility organics in the atmosphere, Atmos. Environ., 42, 3593-3624, 2008.

568 Kurtén, T., Rissanen, M. P., Mackeprang, K., Thornton, J. A., Hyttinen, N., Jørgensen, S., Ehn,
569 M., and Kjaergaard, H. G.: Computational study of hydrogen shifts and ring-opening
570 mechanisms in α-pinene ozonolysis products, J. Phys. Chem. A, 119, 11366-11375, 2015.

571 Lambe, A., Massoli, P., Zhang, X., Canagaratna, M., Nowak, J., Daube, C., Yan, C., Nie, W.,
572 Onasch, T., Jayne, J., Kolb, C., Davidovits, P., Worsnop, D., and Brune, W.: Controlled nitric

oxide production via O(^{1}D) + N$_2$O reactions for use in oxidation flow reactor studies, Atmos. Meas. Tech., 10, 2283-2298, 10.5194/amt-10-2283-2017, 2017.

Liu, Y. J., Herdlinger-Blatt, I., McKinney, K. A., and Martin, S. T.: Production of methyl vinyl ketone and methacrolein via the hydroperoxyl pathway of isoprene oxidation, Atmos. Chem. Phys., 13, 5715-5730, 2013.

Loza, C. L., Craven, J. S., Yee, L. D., Coggon, M. M., Schwantes, R. H., Shiraiwa, M., Zhang, X., Schilling, K. A., Ng, N. L., and Canagaratna, M. R.: Secondary organic aerosol yields of 12-carbon alkanes, Atmos. Chem. Phys., 14, 1423-1439, 2014.

McVay, R. C., Zhang, X., Aumont, B., Valorso, R., Camredon, M., La, Y. S., Wennberg, P. O., and Seinfeld, J. H.: SOA formation from the photooxidation of α-pinene: systematic exploration of the simulation of chamber data, Atmos. Chem. Phys., 16, 2785-2802, 2016.

Miyoshi, A., Hatakeyama, S., and Washida, N.: OH radical-initiated photooxidation of isoprene: An estimate of global CO production, J. Geophys. Res. Atmos., 99, 18779-18787, 1994.

Nah, T., McVay, R. C., Zhang, X., Boyd, C. M., Seinfeld, J. H., and Ng, N. L.: Influence of seed aerosol surface area and oxidation rate on vapor wall deposition and SOA mass yields: a case study with α-pinene ozonolysis, Atmos. Chem. Phys., 16, 9361-9379, 2016.

Ng, N. L., Chhabra, P. S., Chan, A. W. H., Surratt, J. D., Kroll, J. H., Kwan, A. J., McCabe, D. C., Wennberg, P. O., Sorooshian, A., and Murphy, S. M.: Effect of NO$_x$ level on secondary organic aerosol (SOA) formation from the photooxidation of terpenes, Atmos. Chem. Phys., 7, 5159-5174, 2007.

Nguyen, T. B., Crounse, J. D., Schwantes, R. H., Teng, A. P., Bates, K. H., Zhang, X., St Clair, J. M., Brune, W. H., Tyndall, G. S., and Keutsch, F. N.: Overview of the Focused Isoprene eXperiment at the California Institute of Technology (FIXCIT): mechanistic chamber studies on the oxidation of biogenic compounds, Atmos. Chem. Phys., 14, 13531-13549, 2014.

Nguyen, T. B., Bates, K. H., Crounse, J. D., Schwantes, R. H., Zhang, X., Kjaergaard, H. G., Surratt, J. D., Lin, P., Laskin, A., and Seinfeld, J. H.: Mechanism of the hydroxyl radical oxidation of methacryloyl peroxynitrate (MPAN) and its pathway toward secondary organic aerosol formation in the atmosphere, Phys. Chem. Chem. Phys., 17, 17914-17926, 2015.

Orlando, J. J., and Tyndall, G. S.: Laboratory studies of organic peroxy radical chemistry: an overview with emphasis on recent issues of atmospheric significance, Chemical Society Reviews, 41, 6294-6317, 2012.

Paulson, S. E., and Seinfeld, J. H.: Development and evaluation of a photooxidation mechanism for isoprene, J. Geophys. Res. Atmos., 97, 20703-20715, 1992.

Peeters, J., Müller, J.-F. o., Stavrakou, T., and Nguyen, V. S.: Hydroxyl radical recycling in isoprene oxidation driven by hydrogen bonding and hydrogen tunneling: The upgraded LIM1 mechanism, J. Phys. Chem. A, 118, 8625-8643, 2014.

Petropavlovskikh, I., Shetter, R., Hall, S., Ullmann, K., and Bhartia, P. K.: Algorithm for the charge-coupled-device scanning actinic flux spectroradiometer ozone retrieval in support of the Aura satellite validation, Journal of Applied Remote Sensing, 1, 013540-013540-013522, 2007.

Riva, M., Budisulistiorini, S. H., Chen, Y., Zhang, Z., D'Ambro, E. L., Zhang, X., Gold, A., Turpin, B. J., Thornton, J. A., and Canagaratna, M. R.: Chemical Characterization of Secondary

Organic Aerosol from Oxidation of Isoprene Hydroxyhydroperoxides, Environ. Sci. Technol., 50, 9889-9899, 2016.

Rivera-Rios, J. C., Nguyen, T. B., Crounse, J. D., Jud, W., St Clair, J. M., Mikoviny, T., Gilman, J. B., Lerner, B. M., Kaiser, J. B., and Gouw, J. d.: Conversion of hydroperoxides to carbonyls in field and laboratory instrumentation: Observational bias in diagnosing pristine versus anthropogenically controlled atmospheric chemistry, Geophys. Res. Lett., 41, 8645-8651, 2014.

Rollins, A. W., Browne, E. C., Min, K. E., Pusede, S. E., Wooldridge, P. J., Gentner, D. R., Goldstein, A. H., Liu, S., Day, D. A., and Russell, L. M.: Evidence for NOx control over nighttime SOA formation, Science, 337, 1210-1212, 2012.

Ruppert, L., and Becker, K. H.: A product study of the OH radical-initiated oxidation of isoprene: Formation of C 5-unsaturated diols, Atmos. Environ., 34, 1529-1542, 2000.

Schilling Fahnestock, K. A., Yee, L. D., Loza, C. L., Coggon, M. M., Schwantes, R., Zhang, X., Dalleska, N. F., and Seinfeld, J. H.: Secondary organic aerosol composition from C12 alkanes, J. Phys. Chem. A, 119, 4281-4297, 2014.

Schwantes, R. H., Teng, A. P., Nguyen, T. B., Coggon, M. M., Crounse, J. D., St. Clair, J. M., Zhang, X., Schilling, K. A., Seinfeld, J. H., and Wennberg, P. O.: Isoprene NO3 Oxidation Products from the RO2+ HO2 Pathway, J. Phys. Chem. A, 119, 10158-10171, 2015.

Schwantes, R. H., McVay, R. C., Zhang, X., Coggon, M. M., Lignell, H., Flagan, R. C., Wennberg, P. O., and Seinfeld, J. H.: Science of the Environmental Chamber, Advances in Atmospheric Chemistry, 1, 1-93, 2017.

Shilling, J. E., Chen, Q., King, S. M., Rosenoern, T., Kroll, J. H., Worsnop, D. R., McKinney, K. A., and Martin, S. T.: Particle mass yield in secondary organic aerosol formed by the dark ozonolysis of α-pinene, Atmos. Chem. Phys., 8, 2073-2088, 2008.

Shilling, J. E., Zaveri, R. A., Fast, J. D., Kleinman, L., Alexander, M. L., Canagaratna, M. R., Fortner, E., Hubbe, J. M., Jayne, J. T., and Sedlacek, A.: Enhanced SOA formation from mixed anthropogenic and biogenic emissions during the CARES campaign, Atmos. Chem. Phys., 13, 2091-2113, 2013.

Singh, H. B., and Hanst, P. L.: Peroxyacetyl nitrate (PAN) in the unpolluted atmosphere: An important reservoir for nitrogen oxides, Geophys. Res. Lett., 8, 941-944, 1981.

Sprengnether, M., Demerjian, K. L., Donahue, N. M., and Anderson, J. G.: Product analysis of the OH oxidation of isoprene and 1, 3-butadiene in the presence of NO, J. Geophys. Res. Atmos., 107, 2002.

Surratt, J. D., Chan, A. W. H., Eddingsaas, N. C., Chan, M., Loza, C. L., Kwan, A. J., Hersey, S. P., Flagan, R. C., Wennberg, P. O., and Seinfeld, J. H.: Reactive intermediates revealed in secondary organic aerosol formation from isoprene, Proc. Natl. Acad. Sci. USA, 107, 6640-6645, 2010.

Teng, A. P., Crounse, J. D., and Wennberg, P. O.: Isoprene peroxy radical dynamics, J. Am. Chem. Soc., 139, 5367-5377, 2017.

Tuazon, E. C., and Atkinson, R.: A product study of the gas-phase reaction of Isoprene with the OH radical in the presence of NOx, Int. J. Chem. Kinet., 22, 1221-1236, 1990.

654 Wennberg, P. O., Bates, K. H., Crounse, J. D., Dodson, L. G., McVay, R. C., Mertens, L. A.,
655 Nguyen, T. B., Praske, E., Schwantes, R. H., Smarte, M. D., St Clair, J. M., Teng, A. P., Zhang,
656 X., and Seinfeld, J. H.: The gas-phase reactions of isoprene and its major oxidation products,
657 Chem. Rev., under review, 2017.

658 Xu, L., Guo, H., Boyd, C. M., Klein, M., Bougiatioti, A., Cerully, K. M., Hite, J. R., Isaacman-
659 VanWertz, G., Kreisberg, N. M., and Knote, C.: Effects of anthropogenic emissions on aerosol
660 formation from isoprene and monoterpenes in the southeastern United States, Proc. Natl. Acad.
661 Sci. USA, 112, 37-42, 2015.

662 Zhang, X., and Seinfeld, J. H.: A functional group oxidation model (FGOM) for SOA formation
663 and aging, Atmos. Chem. Phys., 13, 5907-5926, 2013.

664 Zhang, X., Cappa, C. D., Jathar, S. H., McVay, R. C., Ensberg, J. J., Kleeman, M. J., and
665 Seinfeld, J. H.: Influence of vapor wall loss in laboratory chambers on yields of secondary
666 organic aerosol, Proc. Natl. Acad. Sci. USA, 111, 5802-5807, 2014a.

667 Zhang, X., Schwantes, R. H., Coggon, M. M., Loza, C. L., Schilling, K. A., Flagan, R. C., and
668 Seinfeld, J. H.: Role of ozone in SOA formation from alkane photooxidation, Atmos. Chem.
669 Phys., 14, 1733-1753, 2014b.

670 Zhang, X., McVay, R. C., Huang, D. D., Dalleska, N. F., Aumont, B., Flagan, R. C., and
671 Seinfeld, J. H.: Formation and evolution of molecular products in α-pinene secondary organic
672 aerosol, Proc. Natl. Acad. Sci. USA, 112, 14168-14173, 2015a.

673 Zhang, X., Schwantes, R. H., McVay, R. C., Lignell, H., Coggon, M. M., Flagan, R. C., and
674 Seinfeld, J. H.: Vapor wall deposition in Teflon chambers, Atmos. Chem. Phys., 15, 4197-4214,
675 2015b.

676 Zhang, X., Lambe, A. T., Upshur, M. A., Brooks, W. A., Gray Bé, A., Thomson, R. J., Geiger, F.
677 M., Surratt, J. D., Zhang, Z., and Gold, A.: Highly Oxygenated Multifunctional Compounds in α-
678 Pinene Secondary Organic Aerosol, Environ. Sci. Technol., 51, 5932-5940, 2017.

679 Ziemann, P. J., and Atkinson, R.: Kinetics, products, and mechanisms of secondary organic
680 aerosol formation, Chemical Society Reviews, 41, 6582-6605, 2012.
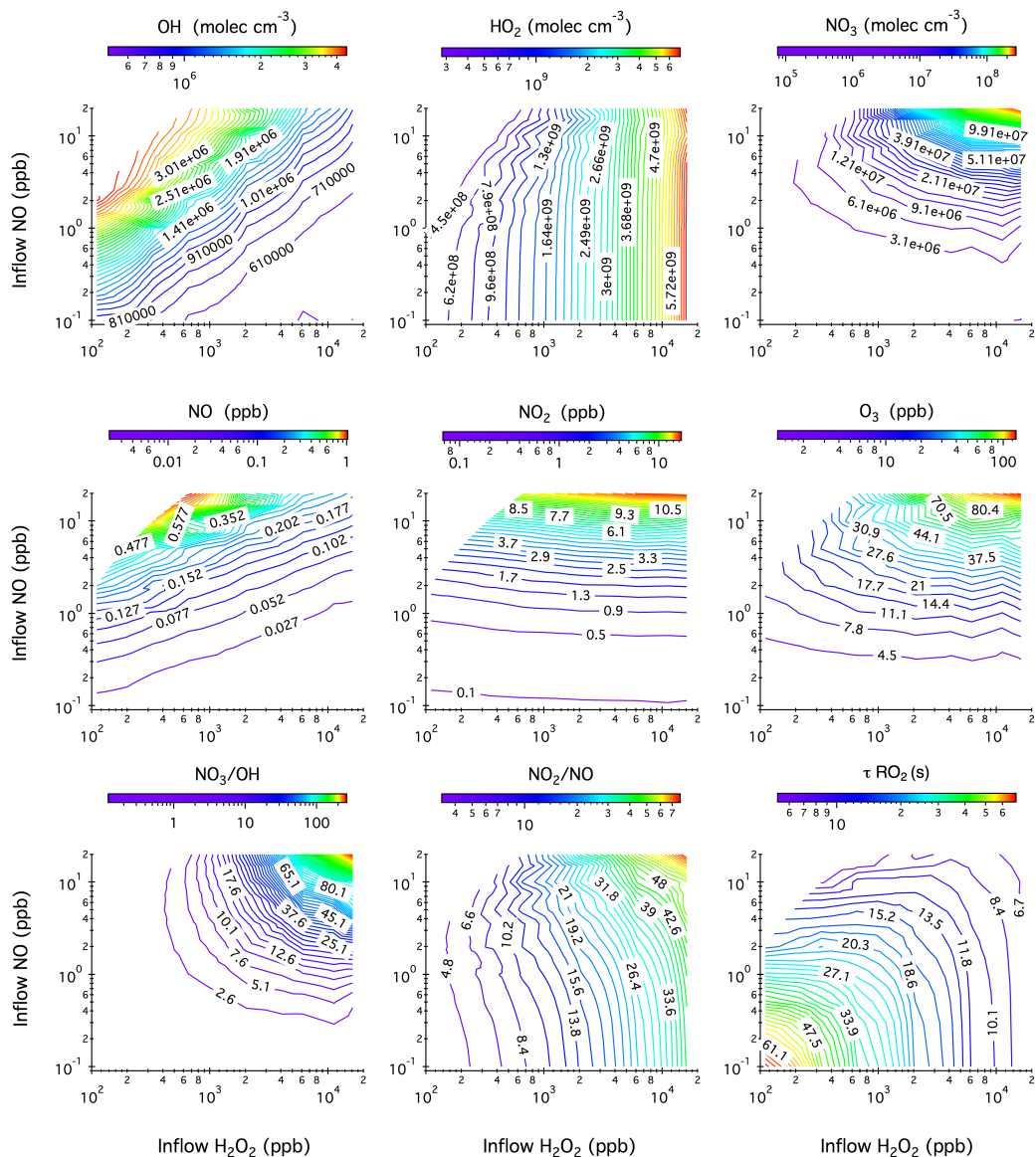
Figure 1. Contour plots showing the model predicted steady-state mixing ratios of OH, HO$_2$, NO$_3$, NO, NO$_2$, and O$_3$ after 20 hours of photochemical reactions in the chamber as a function of the concentrations of H$_2$O$_2$ and NO in the continuous injection flow. Also given here are the simulated NO$_3$ to OH ratio, NO$_2$ to NO ratio, and the lifetime of an RO$_2$ radical (τ_{RO_2}) with respect to reactions with NO and HO$_2$. Note that the ripples on the contour lines originate from the limited simulation datasets that are used to generate iso-response values.
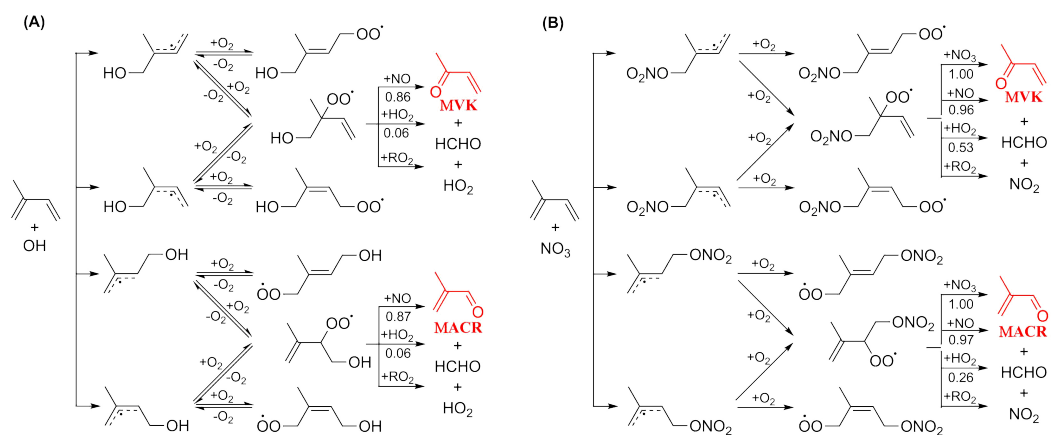
Figure 2. Representative mechanism for (A) OH- and (B) NO$_3$-initiated oxidation of isoprene that leads to the formation of MACR and MVK.
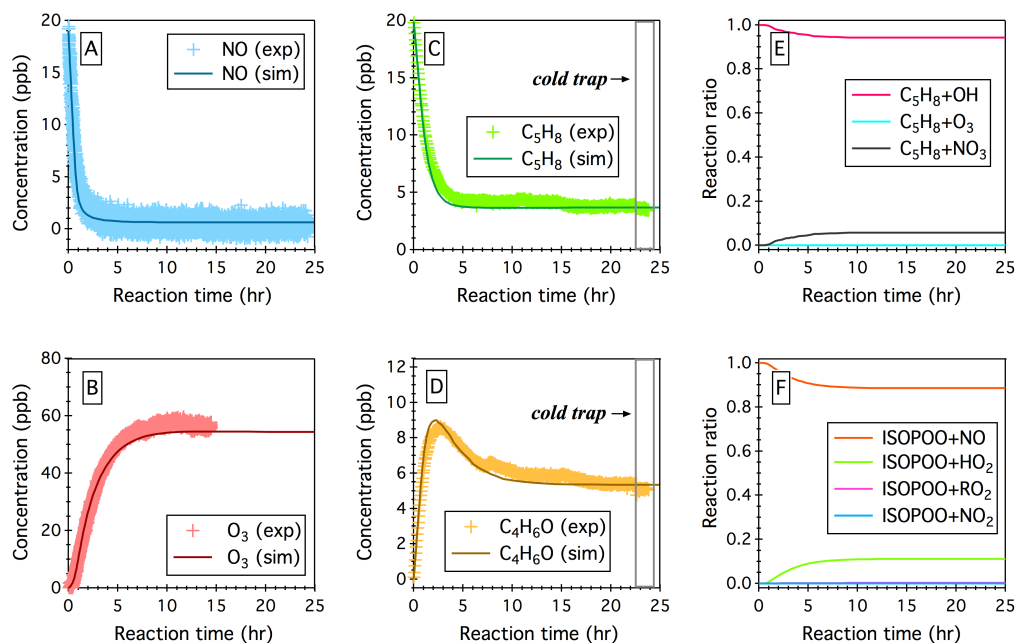
Figure 3. Simulated (sim.) and observed (exp.) temporal profiles of (A) NO, (B) O_3, (C) isoprene (C_5H_8), and (D) the sum of MACR and MVK (C_4H_6O) over 24 hours OH-initiated oxidation of isoprene in the continuous-flow mode chamber operation. Also displayed here include (E) simulated fractions of OH-oxidation, ozonolysis, and NO_3-oxidation as the removal pathways of isoprene, and (F) simulated fractions of ISOPOO radicals that react with NO, HO_2, RO_2, and NO_3. Time 0 is the point at which the chamber lights are turned on. Initial experimental conditions are 19 ppb NO, 0 ppb NO_2, 0 ppb O_3, 600 ppb H_2O_2, and 19.9 ppb C_5H_8, with continuous input of 600 ppb H_2O_2, 19 ppb NO, and 19.9 ppb C_5H_8 over the course of 24 hour photochemical reactions.
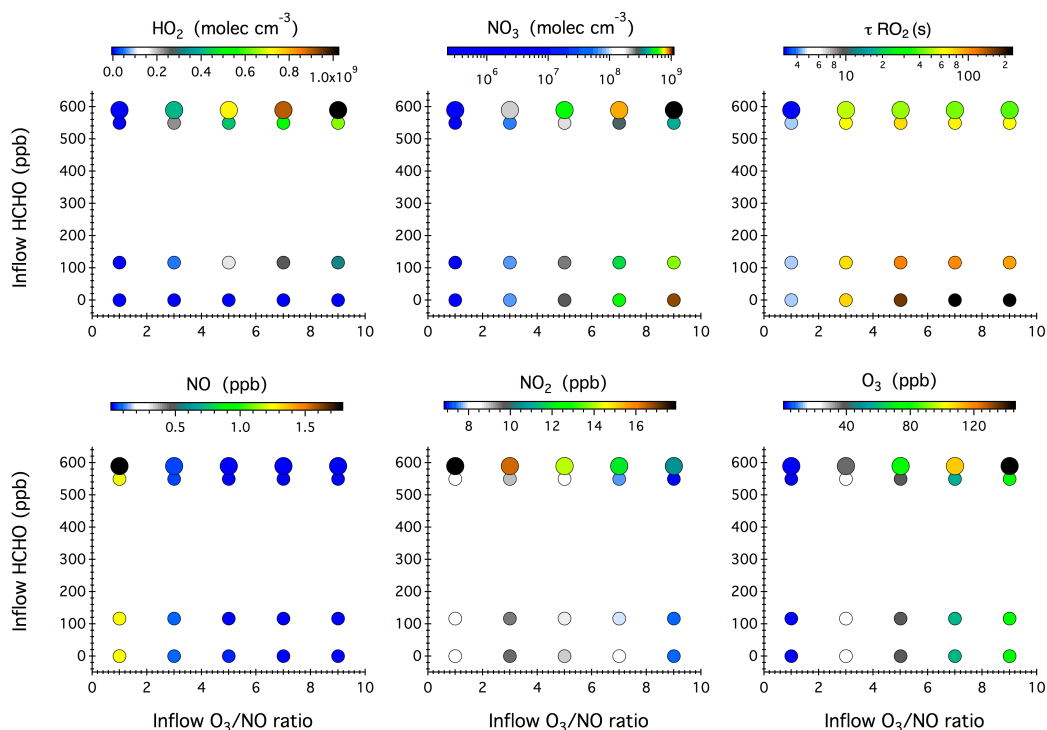
Figure 4. Simulated steady-state mixing ratios of HO_2, NO_3, NO, NO_2, and O_3 after 16 hours of dark reactions in the chamber as a function of the concentrations of NO and O_3 in the continuous injection flow. The symbol size denotes different inflow NO concentrations, i.e., 10 ppb and 20 ppb. Also given here is the calculated lifetime of an RO_2 radical (τ_{RO_2}) with respect to reactions with NO, NO_3, and HO_2.
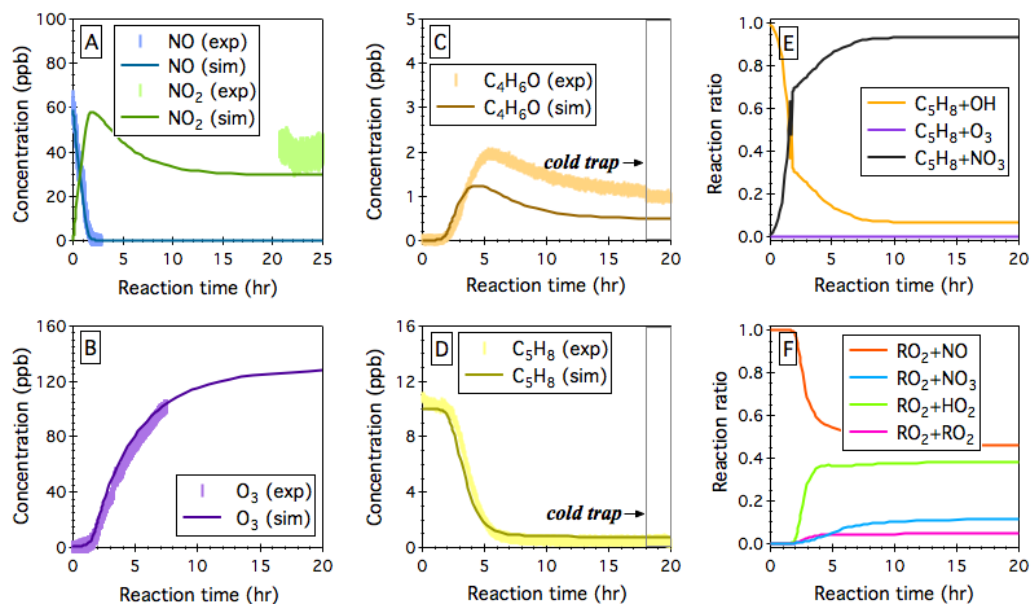
Figure 5. Simulated (sim.) and observed (exp.) evolution patterns of (A) NO_x, (B) O_3, (C) the sum of MACR and MVK (C_4H_6O), and (D) isoprene (C_5H_8) over 25 hours NO_3-initiated oxidation of isoprene under continuous-flow mode chamber operation. The fractions of isoprene that react with OH, O_3, and NO_3 are given in panel (E), and the fractions of INOO radical that undergo bimolecular reactions with NO, NO_3, HO_2, and RO_2 are given in panel (F). Initial experimental conditions are 0 ppb O_3, 59 ppb NO_x, and 10.2 ppb C_5H_8, with continuous input of 205 ppb O_3, 59 ppb NO, and 10.2 ppb C_5H_8 over the course of 25 hour dark reactions.